Open Archive Toulouse Archive Ouverte (OATAO)

OATAO is an open access repository that collects the work of Toulouse researchers and makes it freely available over the web where possible.

This is an author-deposited version published in: http://oatao.univ-toulouse.fr/
Eprints ID: 5464

To link to this article: doi:10.1016/j.ijdevneu.2008.10.006
URL: http://dx.doi.org/10.1016/j.ijdevneu.2008.10.006

To cite this version: Risser, Laurent and Plouraboué, Franck and Cloetens, Peter and Fonta, Caroline (2009) A 3D-investigation shows that angiogenesis in primate cerebral cortex mainly occurs at capillary level. *International Journal of Developmental Neuroscience*, vol. 27 (n° 2). pp. 185-196. ISSN 0736-5748

Any correspondence concerning this service should be sent to the repository administrator: staff-oatao@listes.diff.inp-toulouse.fr

A 3D-investigation shows that angiogenesis in primate cerebral cortex mainly occurs at capillary level

Laurent Risser [a,b], Franck Plouraboué [a], Peter Cloetens [c], Caroline Fonta [d,e,*]

[a] Université de Toulouse, IMFT, UMR5502 CNRS-INPT/UPS, Toulouse, France
[b] CEA/LNAO, Neurospin, Gif-sur-Yvette, France
[c] European Synchrotron Radiation Facility, Grenoble, France
[d] Université de Toulouse, UPS, Centre de Recherche Cerveau et Cognition, France
[e] CNRS, CerCo, Toulouse, France

A B S T R A C T

This paper describes the use of a new 3D high-resolution imaging technique dedicated to functional vessels for a systematic quantitative study of angiogenesis in the primate cortex. We present a new method which permits, using synchrotron X-ray micro-tomography imaging, the identification of micro-vascular components as well as their automatic numerical digitalization and extraction from very large 3D image analysis and post-treatments. This method is used to analyze various levels of micro-vascular organization and their postnatal modifications. Comparing newborn- and adult marmosets, we found an increase in vascular volume (270%), exchange surface (260%) and vessel length (290%) associated to a decrease in distances between vessel and tissue (32%). The increase in relative vascular volumes between the two ages, examined through the whole cortical depth, has been found to be mainly sustained by events occurring at the capillary level, and only marginally at the perforating vessel level. This work shows that the postnatal cortical maturation classically described in terms of synaptogenesis, gliogenesis and connectivity plasticity is accompanied by an intensive remodeling of micro-vascular patterns.

Keywords:
Brain vessels
Micro-vascularization
Postnatal development
Cortical maturation
Primate
Synchrotron micro-tomography
Image segmentation
Skeletonization

1. Introduction

The formation of the cerebral cortex is extremely complex and most of the research efforts have been concentrated on the fate and organization of neuro-ectodermal derived cell types: neurons and, more recently, glial cells. But several investigations are now giving growing evidence that extra elements, namely vessels, may better be considered as important partners in many contexts. Resulting from the effects of evolutionary, physiological and physical constraints, the formation of intra-cortical vasculature is impressively dense and complex. It is becoming an important issue in various clinical or fundamental fields. From the clinical point of view, defaults in the entangled relationship between vascular and neuronal development can lead to various dysfunctions among which brain ischemia, stroke, neuro-degeneration, hypertension (Carmeliet, 2003). In a more fundamental perspective, brain imaging methods which explore brain maturation, aging and pathologies across the lifespan, reflect the complex relationship between cerebral tissue metabolic needs and blood volume, blood flow and oxygen consumption. The spatial resolution limit of NMR, fMRI or PET raises the question of a possible micro-vascular organization at a scale smaller than the resolved one. Deciphering the complexity of the vascular network with a high-resolution preserving the smallest of the capillaries, in a large volume of tissue, appears then as a key point for a better understanding of the neuro-vascular coupling. Moreover, the development of an initial vascularization pattern, triggered by an increase of metabolic needs, as found in tumors or in developing tissue, has hitherto been analyzed in case of pathological angiogenesis but poorly investigated for normal physiological processes of brain postnatal development, the literature relating mainly to early vasculogenesis and prenatal vascularization (Anstrom et al., 2002; Bertossi et al., 1999; Pessacq and Reissenweber, 1972).

Molecular and cellular approaches have dominated the literature in this field. At this point it appears essential to define morphological and topological quantitative parameters characterizing vascular networks, enabling analyses of the effects of various factors in the different steps of angiogenesis, especially in the perspective of anti-angiogenic strategies for tumor therapy. These

* Corresponding author at: CerCo, UMR5549, Faculté de Médecine Rangueil, 31062-Toulouse Cedex 9, France. Tel.: +33 562 172 808; fax: +33 562 172 809.
E-mail address: caroline.fonta@cerco.ups-tlse.fr (C. Fonta).

issues are through-fully discussed in the material and method section of this paper where we propose new systematic tools for a reliable investigation of vascular density in highly complex vascular networks. 3D analyses of large tissue volumes are necessary to obtain reliable data on the organization of vascular networks. Nevertheless most classical studies investigate relative vascular density on two-dimensional images of histological sections. In the last 10 years, methods targeting large cerebral volumes have been developed. Post-mortem methods, such as the corrosion cast technique, provide impressive pictures of the human cortical vasculature using Scanning Electron Microscopy but do not offer the possibility of quantitative analyses (Reina-De La Torre et al., 1998) unless complemented by micro-tomography (Heinzer et al., 2006). More recent techniques such as two-photon microscopy provide powerful in vivo 3D information, they are however restricted by the moderate size of the region of interest as well as obstructed by the shading of upper vessels on lower ones (Nishimura et al., 2007; Stefanovic et al., 2008). High-resolution synchrotron tomography has been proposed for complete 3D imaging of micro-vascular networks with a micrometric resolution inside several cubic millimeters of cerebral tissue and adapted to the analyses of primate vessel networks, as well as to brain tumors in an implanted rat model (Plouraboué et al., 2004; Risser et al., 2007). Such a method not only permits the imaging of very large volume of tissues, but it can also lead to a systematic digitalization of the vessels (Heinzer et al., 2006; Risser et al., 2007). The growing development of focused micro-CT commercial device propounding spatial resolution close to microns also pave the way of a future broader application of the proposed methodology. Beside the possibility of automatic numerical data treatments, the interest of such digitalization is to potentially investigate the relative contribution of small and large vessels on various parameters (e.g. vascular density) during the cortex maturation, so that one can discriminate and analyze the multi-scale organization of the vessel networks.

In this paper we then consider both local and global vascular levels for the investigation of micro-vascular structures development between newborn and adult ages. The motivation of this study is to look for further possible parallel between vascular remodeling and known postnatal neuronal development by performing a systematic 3D quantification. This goal is not only pursued from examining the local vascular relative volume, but also by a detailed comparative investigation of intra-cortical capillaries and perforating vessels networks between newborn and adult monkeys.

2. Materials and methods

2.1. Sample preparation

The analysis was carried out on four marmoset monkeys (*Callithrix jacchus*): two adult males (5 and 6 years old) and two newborns (2 and 3 postnatal days—PND-old, sex undetermined). The animals were from the in-house colony at the accredited primate center of the Centre de Recherche Cerveau et Cognition (CNRS/Université Toulouse, France) and were maintained in accordance with NIH guidelines. The experimental procedures used were carried out in accordance with the recommendations of the EEC (86/609/EEC) and the French National Committee for the use of laboratory animals.

The animals, euthanized by a lethal injection of pentobarbital, were intracardially perfused first by a heparinized solution of 0.9% NaCl, followed by a suspension of barium sulfate 600 mg/ml (Micropaque, Guerbet®). Then the brain was extracted and fixed in a 10% formalin solution. Anatomic landmarks, in particular the lateral sulcus, were used to cut samples in different cortical areas of interest, using a cylindrical biopsy punch (3 mm internal diameter) in the left cerebral hemisphere (Fig. 1A). Each sample was dehydrated and embedded in epoxy resin in a cylindrical mold 6 mm in diameter (Fig. 1B).

The quality of the brain perfusion was assessed from general observation and was completed by a detailed analysis of each sample after micro-tomography imaging (punctual imperfect filling, presence of interruptions in the network, vessels with blunt ends). Almost fifty percent of the samples were discarded because of unsatisfactory contrast agent injection. Although the sample preparation is standardized (Plouraboué et al., 2004), the injection of the contrast agent in the whole vessel network is difficult to achieve in all the animals. If the injection appears regular and complete in some animals, in some other cases, some parts of the brain can be imperfectly filled, maybe due to physiological parameters or variations. We are currently aiming at improving the procedure (e.g. a better control of the contrast agent temperature in order to lower its viscosity). As the impact of our method is highly dependent on the quality of the preparation, our sample selection is demanding and explains the differences in the sample number in each group and the variability between groups. Such requirements limit the perfect match of homologous cortical samples between animals.

A fraction of the samples analyzed in this paper had been used in a previous study analyzing multi-scale properties of normal and tumor vascular networks (Risser et al., 2007). Table 1 summarizes the samples used in this study and their possible contribution to the previous investigations.

2.2. Sample shrinkage

The fixation and embedding protocols resulted in a reduction of the sample volume, that was quantified by calculating the ratio between the initial diameter (3 mm) and the diameters measured from the X-ray images, assuming a homogeneous reduction in the whole sample (Risser et al., 2007). The shrinkage was higher for newborn than for adult brains, with a reduction factor that was, on average, 1.7 times higher for newborn than for adult samples (Table 1). This can be explained by a difference in water content (around 12% difference) between the two tissues.

An important point concerns the size reduction of brain parenchyma on the one hand and vessels on the other hand. Concerning the vessels, we assumed a similar reduction factor for young and adult brain vessels since vessels were filled with the same solution in both groups (600 mg/ml barium sulfate). Furthermore, we conducted parallel experiments, injecting adult brains with a more diluted barium sulfate solution (300 mg/ml) and found that vessel diameters were not different from those injected with a 600 mg/ml solution. With a reduction factor of 1.4 (mean value of tissue reduction factor for adults), vessel diameters presented similar values to those mentioned in the literature, while a reduction factor of 2.4 (consistent with the newborn sample reduction factor) would generate diameter values far below the literature data (data not shown).

Beside parenchyma, vessel walls behave differently in newborn and adults animals due to the difference in structure and composition of their basal laminar contents. Indeed, we found that adult's vessel tortuosity, estimated as in Risser et al. (2008), is much higher for thin vessels that for wide ones (Fig. 2A). We furthermore found a different result in newborn samples: the observed tortuosity in this group is weakly dependent on vessel diameter as illustrated in Fig. 2B. Therefore the maturity of the brain tissue interferes with the shrinkage of its different components. Although the choice of a uniform 1.4 reduction factor in all animals may require more careful inspection, e.g. by performing a rigorous check on vessel diameter and shape at each step of the sample preparation, it has to be clearly stated that the chosen estimation did not interfere with many of the parameters analyzed at present.

2.3. Histology

In order to control the location of the cortical samples so as to identify them, histological checks were performed after sample extraction. The left cerebral hemisphere was cryo-protected in a 30% sucrose solution in phosphate buffer 0.1 M and cut with a freezing microtome. Parasagittal sections (40 μm thick) were stained with Cresyl Violet (Fig. 1C). The position of each sample was identified on the sections and possibly named after cyto-architectonic criteria. For example, sample m51 was extracted from the most occipital part of the primary visual cortex (V1 or Brodman area 17 characterized by a fairly low cell density layer, the stria of Gennari, ending at the boundaries of this area with the surrounding cortex of area 18). It provided 3 sub-samples, m51_4 representing the operculum vascularization (integrating central visual field input), and m51_3 and m51_5 representing the calcarine visual cortex (integrating the peripheral visual field input) (Fig. 1D). Samples that were found to be located on several or undefined areas were named after their positions in the different cerebral lobes (frontal, occipital, temporal, and parietal) (Table 1).

2.4. Image analysis

The samples were imaged with an intense monochromatic and parallel synchrotron X-ray beam at the experimental station ID19 of the European Synchrotron Radiation Facility (ESRF, Grenoble, France) (Plouraboué et al., 2004; Risser et al., 2007). The extremely large data sets generated by the 3D images (4–5 GB of data per image) led us to develop specific numerical approaches for image analysis and data processing.

Gray level images were segmented. Voxels within vessels and voxels within tissue were then distinguished (detailed in Risser et al., 2007). The volumes were rendered using the commercial software Amira® (Mercury, Richmond, TX, USA) (Fig. 1D).

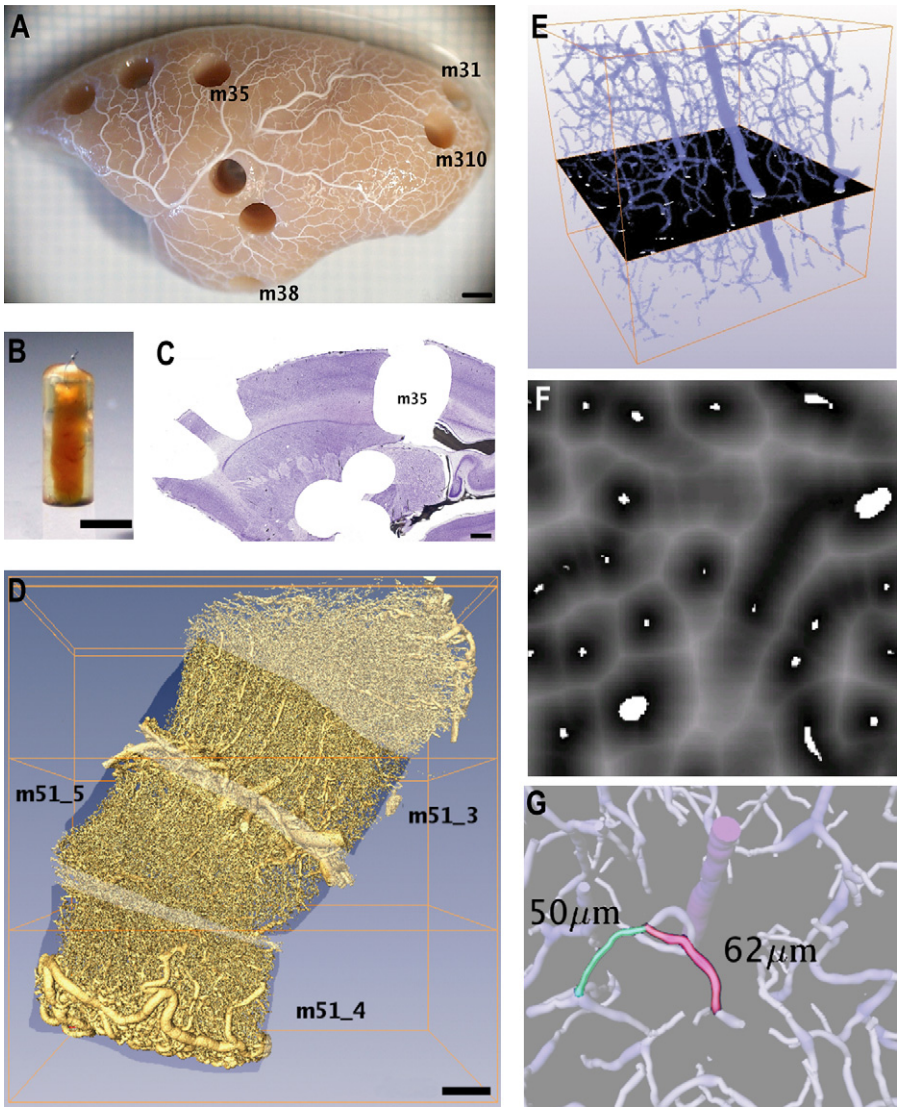

Fig. 1. Sample preparation, imaging and data analysis. (A) Lateral view of an adult marmoset left hemisphere (frontal lobe on the left). After barium sulfate perfusion, brain tissue was fixed and samples (3 mm in diameter) were cut, perpendicularly to the brain surface, in various cortical regions with a biopsy punch. Numbers refer to samples analyzed in this work (*cf.* Table 1). (B) Once dehydrated, each sample was included in epoxy resin (final diameter 6 mm). (C) 40 μm-parasagittal section of the hemisphere shown in (A), stained with Violet Cresyl, to provide neuroarchitectonic information on sample location. (D) Volume rendering of newborn sample m51 (primary visual cortex) comprising operculum (m51_4) and calcarine (m51_3 and m51_5) visual cortex. (E) Slice-by-slice analysis. Vascular volume and distance maps were studied through the cortical depth in successive virtual sections (in black) parallel to the cortical surface and 1.4 μm thick. This analysis was performed in marmoset samples for assessing the laminar organization of the cerebral cortex. (F) Distance map analysis reflecting blood/tissue exchanges. Distances between each point of the tissue and the nearest vessel (either capillary or large-diameter vessel in white) were measured in the whole 3D-sample. Here distance map is presented for one slice, with a gradient from the shortest (black) to the longest (light gray) tissue/vessel distance. (G) Segment length, defined as the distance between two successive branching points, illustrated in 2 examples measuring 50 and 62 μm. Scale bars: 5 mm (A), 6 mm (B), 1000 μm (C), and 300 μm (D).

2.5. Data processing and analyzing

Several parameters are generally considered in the aim of reflecting the notion of vessel density or blood-tissue exchange in the cerebral cortex. This is why many studies have considered the relative evolution of vessel density, by varying age, cellular or molecular contexts (Augustin, 2001; Heinzer et al., 2008; Weber et al., 2008).

There are nevertheless a number of significant drawbacks in such a straightforward analysis. First, very few studies are concerned by the identification of some intrinsic parameter to quantify vessel density. Most studies rather consider a large panel of different analysis protocols for the investigation of a relative vascular density parameter on histological sections such as the number of vascular profiles per unit area (Tuor et al., 1994), the ratio of the area occupied by vessels to the area of interest (Fonta and Imbert, 2002; Michaloudi et al., 2006), the intersections of vessels with a grid (Argandoña and Lafuente, 1996), or the vascular length per unit area or volume (Bell and Ball, 1985; Tieman et al., 2004; Weber et al., 2008). This might not be a serious issue since most studies are more concerned by finding a relative effect associated with different conditions rather than providing some absolute quantification.

There is a second more subtle side effect in most previous analyses associated with statistical variability of the measurements. None of those studies have considered the possible influence of spatial correlation length of the vascular networks on the analyzed volume size. This length gives the typical length-scale for which the spatial distribution of the vascular density can be considered as de-correlated. It is then necessary to investigate a "large" number of such units in order to obtain statistically representative quantities (30 is generally considered as "large" enough to estimate the average value to within 20% of the true value). Below this correlation length, which is estimated at between 50 and 80 μm in rat and primate cortex, cortical vascular networks have a fractal organization, while, beyond the correlation length, vessel networks can be considered as homogeneous (Risser et al., 2007). This correlation length also gives the typical size above which one could define a vascular organization module. It is indeed smaller than the typical distance between arteriole and vein columns (also named perforating vessels after Marin-Padilla, 1988) as further analyzed in this paper.

Hence the major drawback of any local quantification of vascular density is to ignore the existence and possible modifications of vessel organization at a broader scale which might be physiologically more important than possibly fluctuating

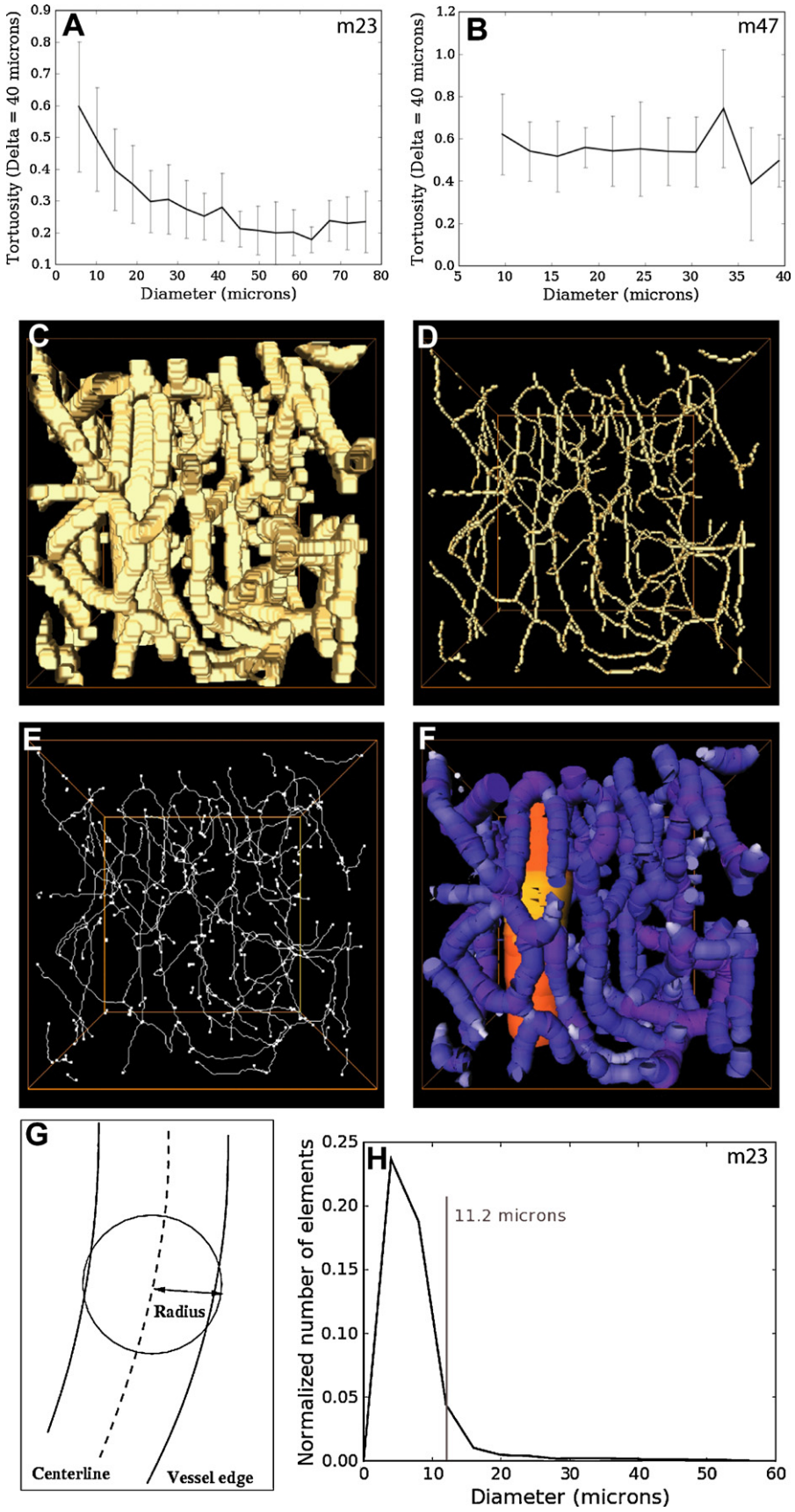

Fig. 2. Data processing. (A and B) Tortuosity, measured as the mean angle between two successive vessel parts (each part = 40 μm, detailed in Risser et al., 2008), is clearly smaller for large vessels than for thin ones in adult monkey (A). This phenomenon is not observed in neonates (B). (C–F) Procedure of vessel skeletonization: considering a binarized 3D image of vascular network volume rendering, the vascular structure boundaries are iteratively eroded (D) until only their centrelines are left. After this erosion

Table 1
List and main characteristics of the samples studied.

Origin	Sample	Localisation	Sample size mm^3	Reduction factor	Nb perforating vessels/mm^2	Nb segments/mm^3 (% large vessel segments)
Adult monkey, 5 years	m23 *(M1)*	Motor cortex	8.58	1.42	9.89	5195 (46.12)
	m26 *(M2)*	Extrastriate visual cortex	0.66	1.36	11.5	8108 (24.07)
Adult monkey, 6 years	m31	Visual cortex (areas 17/18)	2.01	1.21	13.7	9140 (39.31)
	m35 *(M4)*	Somatosensory/motor cortex	6.71	1.4	9.68	6158 (28.47)
	m38 *(M5)*	Infero-temporal cortex	5.45	1.4	8.44	7615 (37.03)
	m310	Primary visual cortex (calcarine)	2.73	1.36	15.0	4991 (30.19)
Newborn monkey, 2 PND	m45	Somatosensory cortex	7.13	2.6	10.6	4467 (54.38)
	m46	Frontal cortex	5.71	2.38	9.04	4399 (69.83)
	m47	Frontal cortex	3.27	2	10.2	4284 (47.63)
Newborn monkey, 3 PND	$m51_{\_3}$	Primary visual cortex	3.13	2.38	12.5	2970 (51.90)
	$m51_{\_4}$	Primary visual cortex	0.58	2.38	15.7	6569 (73.31)
	$m51_{\_5}$	Primary visual cortex	1.23	2.38	9.55	3104 (50.43)
	m55	Somatosensory cortex	8.07	2.1	8.67	2208 (37.48)
	m59	Extrastriate visual cortex	2.64	2.3	7.84	3473 (55.19)
	m510	Parietal cortex	6.00	2.7	6.58	1844 (42.21)

Italics: corresponding nomenclature used in Risser et al. (2007). A segment (right column) is defined as the part of vessel between two successive branching points.

local modifications as pointed out by Augustin (2001). This point is crucial since the presence of vessels is not a priori directly related to any functional role (Heinzer et al., 2008).

Investigating our large-sized-samples, we chose several parameters to provide objective information on the vessel networks, from a first step which is associated with the digitalization of the vessel's skeleton.

2.5.1. Network skeletonization

The skeleton of a vessel-like shape is the ordered set of the points which define its centerlines. Local vessel radius is moreover associated to each centerline point. The skeleton representation of a vessel-like shape is then optimal for analysis purpose since it only contains useful and directly interpretable information (Fig. 2C–F). Skeletonization was performed, in this study, using the algorithm proposed by Palágyi and co-workers (Palágyi et al., 2001; Risser et al., 2008). Radius estimates after skeletonization were not similar to those observed in the original images. Therefore a post-treatment was carried out to provide accurate evaluations of the vessel radii. Around each point of the vessel centerline, a sphere was expanded until 10% of its volume was left outside the vessel shape in the segmented image (Fig. 2G). This percentage was chosen empirically to provide the best radii estimates when the skeletons and original images are superposed. Slight variations around this percentage induced very few changes in the estimated radius values.

2.5.2. Vessel classification and notion of segment

2.5.2.1. Vessel classification. Considering the whole range of vessel diameter values, we observed a cut-off in the distribution around 11.2 μm (Fig. 2H) in all adult samples which allowed to choose this value as a threshold to discriminate large- and small-diameter vessels, the last ones being considered as capillaries (Bell and Ball, 1985; Cassot et al., 2006). Such a classification corresponds to a physiological partition since large vessels are essentially involved in the regional control of blood flow, though recent data put forward the contribution of small-diameter vessels to blood flow regulation (Mulligan and MacVicar, 2004; Peppiatt et al., 2006). Nevertheless capillaries represent the actual site for oxygen, nutrient and exogenous molecules delivery.

2.5.2.2. Segments. A segment is defined as a part of the vascular network between two bifurcations, between a bifurcation and a non-connected segment-end or between two non-connected segment-ends (Fig. 1G). The two latter cases might be due to imperfect injection in the vascular network and were discarded from the analysis. Segment lengths are evaluated by summing the distances between their successive points of the skeletonized network. The number of segments obtained for each sample is indicated in Table 1.

2.5.3. Vascular length and surface

Vascular length refers to the sum of segment lengths within a region of interest (ROI). Similarly, segment surface estimates are the sum of cylinder surfaces whose axes are the successive segment points and radii the averaged radius between two corresponding successive points.

2.5.4. Global and slice-by-slice analysis: vessel density and mean-distance-to-a-vessel analysis

2.5.4.1. Global and slice-by-slice analysis. Relative vascular volume and mean distance to a vessel were studied on whole sample volumes as well as through the cortical depth of the gray matter. For the study through the cortical depth, samples were subdivided into thin slices parallel to the cortical surface (Fig. 1E). Slices were 1.4 μm thick, which corresponds to the image resolution. The vessel density and the mean distance to a vessel were then computed inside each slice, taking the slice depth into account.

2.5.4.2. Relative vascular volume. In a region of interest, this value was computed as the portion of voxels considered in the vascular network over the total number of voxels.

2.5.4.3. Mean distance to a vessel. Mean distance to a vessel estimations were performed using distance maps. These maps express, at each of their points, the Euclidian distance to the nearest vessel in a corresponding segmented image ROI. Distance maps were computed using a simple distance propagation algorithm. Mean distances to nearest vessel were computed as the distance map mean value in ROIs. Analyses through the cortical depth were performed from each slice of the computed 3D-distance map (Fig. 1F).

2.6. Statistics

We used the non-parametric Kruskal–Wallis statistical test, for each parameter studied on the different samples. *P* values lower than 0.05 were taken to indicate significant differences. We used a classical Quantile–Quantile plot representation to test the possible Gaussian distribution of the large vessel number in samples. We also performed a rank test for cumulative density distribution to test the Gaussian distribution.

3. Results

We first present the results obtained for the adult micro-vascular networks and then compare them to newborn's ones.

3.1. Characterization of vessel networks in adult monkey

The *vascular volume* inside the gray matter represents from 2 to 4.3% of the total volume in the different adult marmoset samples, a

step, the centreline voxels are ordered as segments (E) and a radius is associated to each of the centreline voxels ((F) color-coded representation of the radius value from blue (capillaries) to yellow-orange (large vessels)). (G) The skeletonization algorithm generates an imprecise evaluation of vessel radius and needs to be improved by a post-treatment procedure. From the coordinates of each skeleton element, a sphere volume is increased until 90% of its points are contained inside the vessel. The value of the corresponding radius is then calculated. (H) The histogram of vessel diameters peaks at around 5 μm, decreases rapidly then slopes gently down. We splitted the vessel population into 2 groups using a threshold at the diameter of 11.2 μm where the histogram behavior changes. Vessels below this threshold mainly correspond to capillaries. (For interpretation of the references to color in this figure legend, the reader is referred to the web version of the article.)

Table 2
Vessel density and morphometry (data and statistics).

Sample	Vascular volume $\times 10^{-2}$ (mm^3/mm^3)	Slope vascular volume $\times 10^{-4}$	Mean ratio large/all vessels	Slope large/all vessels $\times 10^{-4}$	Surface (mm^2/mm^3)	Vascular length (mm/mm^3)	Segment length (μm)	Slope segment length	Mean diameter (μm)	Mean large vessel diameter (μm)
Adults										
m23	3.19	−6.1	0.48	−1.25	8.85	288	98.0	−0.0102	9.88	14.97
m26	2.09	−8.5	0.23	−3.85	8.16	310	94.3	−0.0106	8.34	14.70
m31	4.30	−27.0	0.45	−3.91	11.32	377	92.5	−0.0108	9.62	14.85
m35	2.02	−13.0	0.50	−1.56	5.58	202	86.2	−0.0116	9.10	15.88
m38	2.81	−16.0	0.43	−2.06	7.99	265	87.7	−0.0114	9.71	15.50
m310	2.08	0	0.56	−4.85	5.32	177	86.2	−0.0116	9.72	15.29
Nborns										
m45	1.61	−4.3	0.52	−0.93	4.06	116	53.4	−0.0187	10.97	15.05
m46	1.06	0	0.48	0.86	2.91	82	56.1	−0.0178	11.14	15.42
m47	1.58	−6.0	0.42	0	4.83	157	59.1	−0.0169	9.70	14.38
m51_3	0.92	7.5	0.37	−1.17	3.05	97	71.4	−0.0140	10.00	14.00
m51_4	1.62	−8.9	0.36	−2.66	5.01	143	53.1	−0.0188	11.40	14.83
m51_5	0.67	0	0.47	−3.52	2.08	69	75.7	−0.0132	9.87	15.13
m55	0.75	−2.4	0.41	−1.09	2.45	82	76.9	−0.0130	9.60	15.55
m59	0.55	−3.3	0.46	−1.5	1.54	44	71.4	−0.0140	10.70	16.02
m510	0.45	−3.4	0.37	−2.39	1.48	48	74	−0.0135	9.68	14.86
P values, adult/Nborn	0.00146	0.9059	0.3759	0.04513	0.00146	0.00145	0.00143	0.00112	0.05935	0.515

variation that may be linked to the cortical area under consideration (Table 2). For example the opercular visual cortex (m31) appears strongly vascularized in comparison with the visual cortex of the calcarine sulcus (m310).

The relative contribution of large-diameter vessels (more than 11.2 μm in diameter) to the vascular volume was, on average, 44% of the vascular volume in adult marmosets. Thus, about 60% of the blood volume perfusing the cortical tissue is found in capillaries (Table 2, Fig. 4A). It is therefore essential to determine how these two types of vessels contributed to the vascular volume through the cortical depth (Fig. 3A–C). As shown in Fig. 3G and H, the relative vascular volume (black line) reflects the vascular volume attributed to the large-diameter vessels (blue line) and the volume attributed to the capillaries (red line). In fact, the proportion of large vessels decreased linearly through the cortical depth (Fig. 3D). This quantitative result agrees well with the qualitative description of the perforating vessels inside the cortex, which present various degrees of penetration, some extending to the white matter, others reaching the lower and middle layers or limited in their penetration to superficial layers in humans (Duvernoy et al., 1981). Unlike the large vessel contribution, the capillary relative volume does not vary much in the whole cortical depth (Fig. 3F). Hence, although the global vascular relative volume varies markedly inside the gray matter, the cerebral tissue may be homogeneously blood-supplied since exchanges between blood and cerebral tissue essentially occur at the capillary level.

However, vessel density is highly dependent on the reduction factor that is applied to the vessels through the experimental procedures. Vascular volumes may present variations of high amplitude related to small variations of the reduction factor. Volume variations are indeed related to reduction factor variations with a polynomial relation of order 3. While in our experimental design the reduction of vessel shrinkage is hypothesized, reduction of cortical tissue has been measured (as explained in Section 2). Therefore the *distance* between any point of the cortical parenchyma and the nearest vessel appears as a more reliable parameter to quantify vessel density. Three distances were estimated: first, the distance to any small vessel, since this distance determines the extent of exchanges between blood and tissue; second, the distance to any large vessel as this distance provides information about the size of the large vessels' vascular territories; third, the distance to any vessel, so as to be able to estimate the relative impact of large and small vessels on this new parameter of vascular density quantification (Table 3).

The mode of the distance to any vessel is extremely similar to that evaluated for the distance to any small-diameter vessel, from one sample to another and is very close to the corresponding average distance. Furthermore, the mode of large vessel distance distribution was found to be much higher and more variable from sample to sample, closely following the corresponding averaged distance. From these observations, we conclude that the vessel density that can be estimated from the distance map is much less sensitive to large vessel contributions than the relative vessel volume.

We subsequently examined the variation of the distance to any vessel or to a large vessel through the cortical depth. These distances varied almost linearly within the cortex depth, allowing the comparison to be made among mean distances (Table 3). The average distance between any point of the cerebral tissue and the nearest vessel was 26.8 μm (±3.8 μm) for adult marmoset. The average distance to a large vessel was 177 μm (±17.7 μm) (Fig. 4C and D).

It is interesting to compare this capillary perfusion typical length-scale with the typical vessel length between two bifurcations in the capillary network. The characteristic *segment length* was found to be 90.8 μm (±4.8 μm) for adult marmoset samples and did not vary much among different samples (Table 2, Fig. 4B).

The description of the vascular network in relation with the cortical tissue was completed by the measurements of *vessel surface areas* (representing the exchange surface area between blood and brain parenchyma) and *vessel lengths* (indicative of vessel trajectories inside the tissue). On average, nearly 8 mm^2 of vessels were in contact with tissue inside 1 mm^3 of brain, and 28 cm of vessels irrigated 1 mm^3 of tissue (Table 2, Fig. 4E and F).

3.2. Postnatal development of cortical vasculature in the marmoset

From a qualitative point of view, the general aspect of the vessel network appeared similar in newborns and in adults, with large vessels perforating the cortical tissue from the brain surface and a dense penetrating network of capillaries inside the whole of the gray matter thickness (Fig. 5A and B).

Comparing the values of different morphometric parameters between the two ages, we generally found significant differences,

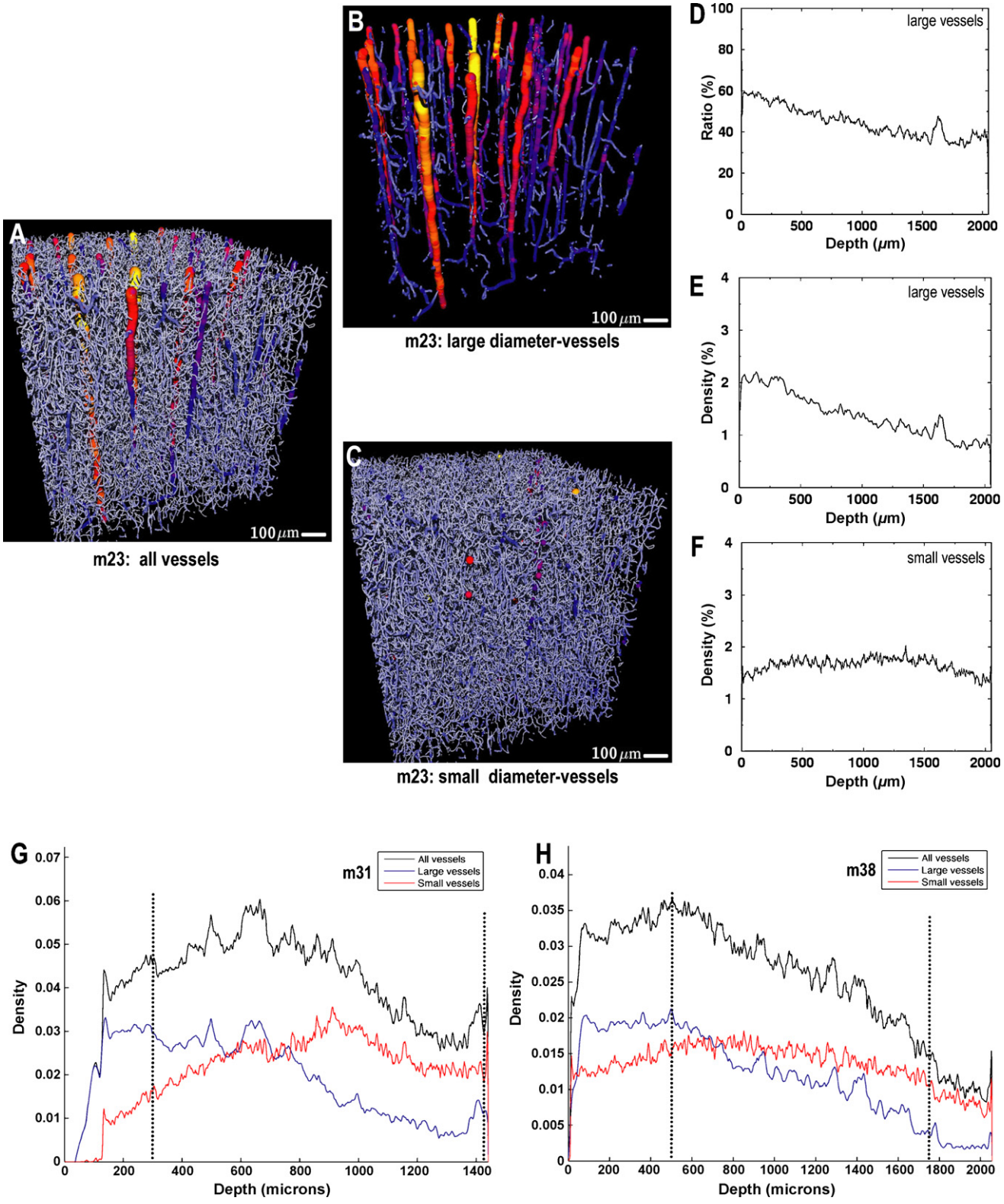

Fig. 3. Contributions of large- and small-diameter-vessels to the vascular volume through the cortical depth. The percentage of large vessels (diameter greater than 11.2 μm (B)) decreases through the cortical depth, as does the large-vessel vascular volume (D, E, G, and H). Comparatively, variation of small-vessel vascular volume (diameter inferior to 11.2 μm (C)) through the cortical thickness is small (F and H) but can display larger amplitudes in sensory cortex (G). Vessel density variation might be characteristic of the cortex function. In sensory areas (m31 (G)) the relative vascular volume increases then decreases from the top to the lowest part of the gray matter, while in samples taken from integration (m38 (H)) or motor (m23 (A–F)) areas, the density decreases regularly through the cortical depth. Dotted lines in (G) and (H) indicate the upper (left) and lower (right) limits of cortical thickness.

Table 3
Distance maps (data and statistics).

Sample	Mode of distance map histogram (μm)			Mean distance/ any vessel (μm)	Slope (any vessel) $\times 10^{-3}$	Mean distance/ large vessel (μm)	Slope (large vessel) $\times 10^{-2}$
	Any vessel	Large vessel	Small vessel				
Adults							
m23	22	140	22	24	2.5	165	4.0
m26	21	190	21	24	5.0	205	8.0
m31	19	125	19	24	0	180	14.0
m35	25	155	25	30	8.0	180	5.0
m38	22	140	22	26	6.0	152	10.0
m310	25	120	25	33	−15.0	180	15.0
Newborns							
m45	26	120	26	28	2.5	126	6.0
m46	34	170	34	36	−2.5	177	−5.0
m47	25	180	25	32	3.10	150	4.0
m51_3	32	175	32	35	−8.0	216	−1.0
m51_4	29	155	29	28	8.0	165	30.0
m51_5	36	140	36	42	−19.0	179	16.0
m55	30	190	30	50	4.0	237	15.0
m59	38	210	38	55	10.0	262	20.0
m510	35	215	35	50	18.0	250	10.0
P values, adult/Nborn	0.00209	0.1094	0.0021	0.009141	0.906	0.7673	0.7677

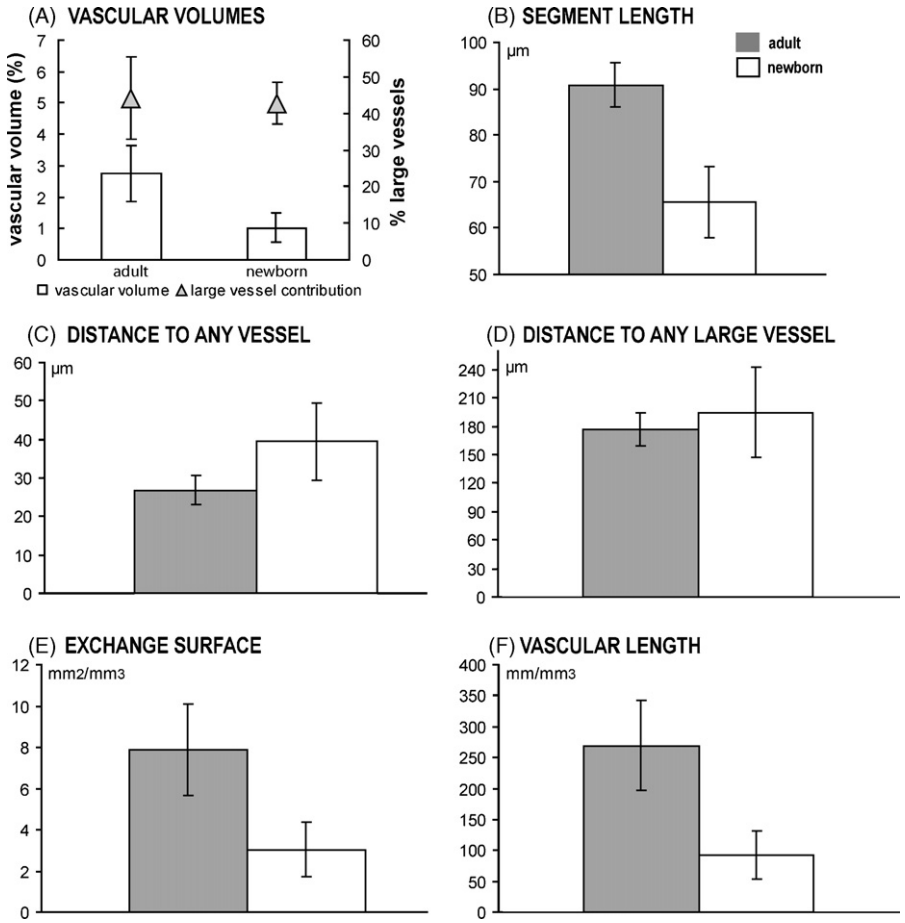

Fig. 4. Comparative data between adult and newborn vessel networks (means and standard deviations). (A) Vascular volume (expressed as vessel volume per 100 mm^3 of tissue) is significantly smaller in newborn than in adult monkeys (~1% versus 2.5%). It is sustained by a predominant contribution of capillaries since 43–44% of the vascular volume correspond to large-diameter vessels in both newborns and adults. (B) The characteristic values for the segment length, around 91 μm in adults and 66 μm in newborn marmosets, are significantly different between the two ages. The classical view of vessel density is counterbalanced by the analysis of distances between vessel and tissue (C and D). In newborns, tissue/vessel distance is significantly larger (~40 μm) than in adult marmosets (~27 μm), when considering any nearest vessel (C). However it is similar for the distance to large-diameter vessels (D). (E and F) Exchange surface area ((E) expressed in mm^2 of vessel surface per mm^3 of tissue) and vascular length ((F) expressed in mm of vessel length per mm^3 of tissue) are significantly different between newborn and adult monkeys.

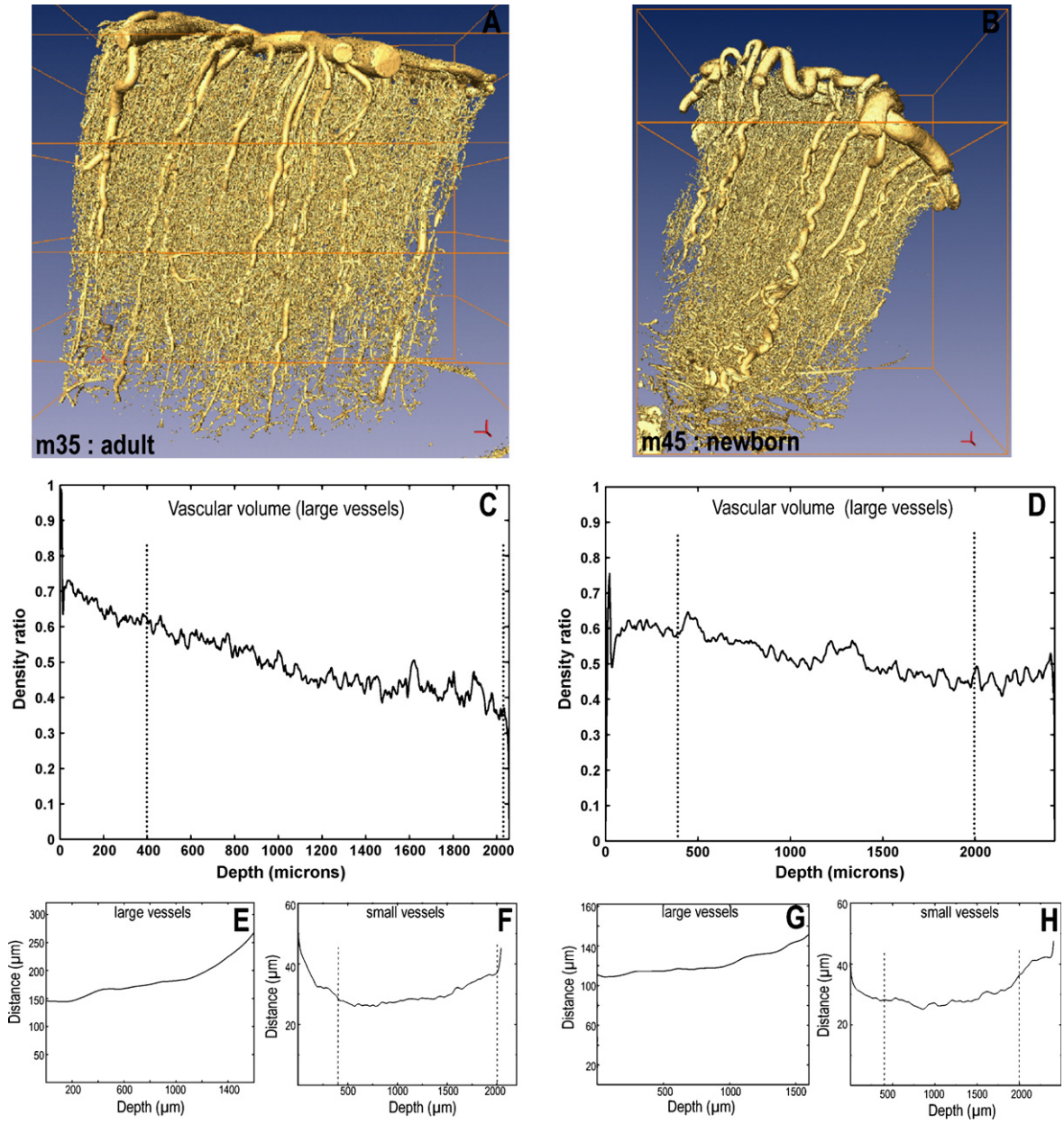

Fig. 5. Comparative analysis of vascular volume and distance map through cortical depth between adult (m35, left) and newborn (m45, right) in similar cortical regions. Vessel patterns are characterized by large perforating vessels perpendicular to the surface, branching into a dense net of smaller vessels spread throughout the tissue volume ((A and B) scale bar: 100 µm). In both samples, the relative vascular volume corresponding to large-diameter vessels decreases through the cortical depth, but with a significantly gentler slope for the newborn (C and D). As the mean contribution of large vessels is similar for newborns and adults (42 and 44%), the contribution of capillaries through the cortical thickness must increase more in adults than in newborns. The distance between tissue and any large vessel increases linearly as a function of cortical depth, with a similar slope for adult and newborns (E and G). Distances to the nearest capillary vary only slightly, with the same amplitude and profile in the two groups (F and H). Dotted lines in (C, D, F, and H) indicate the upper (left) and lower (right) limits of cortical thickness.

which gave an objective description of the vascular network modifications associated with postnatal cortical development.

Relative vascular volume (Fig. 4A), *exchange surface area* (Fig. 4E) and *vascular length* (Fig. 4F) were significantly different between newborn and adult marmosets (Table 2). Mean vascular relative volume and vascular relative surface area in adults ($2.74 \pm 0.89\%$, 7.87 ± 2.22 mm^2/mm^3 respectively) were more than twice those in newborns ($1.02 \pm 0.47\%$ and $3.04 \pm 1.32\%$ respectively), and the vascular length was three times as long (269 ± 73 mm/mm^3 versus 93 ± 39 mm/mm^3).

We also measured the relative *vascular volumes* along the axis perpendicular to the cortical surface in newborns. The slope of the resulting variations obviously varied from sample to sample and was generally negative (Table 2). Although there was a high variability, the values were not significantly different between adults and newborns ($P = 0.9059$). Hence the relative vascular volume is higher in the superficial layers of the cortex and generally decreases through the cortical depth. However, this pattern, already present at birth, might present some specificity since its variations in the cortical depth displayed slopes that were different from one sample to another, reflecting developmental and/or area specificity.

As the mean relative vascular volume increases between newborns and adults, the question arises as to how large and

small vessels contribute to this change since the mean ratio of large to small vessel contributions to vascular volume is similar in adults and newborns (Table 2, Fig. 4A). Actually, the large vessel (diameter greater than 11.2 μm) contribution to the vascular volume represents nearly half of the total vascular volume: 44.1% (±11.3) for adults and 42.8% (±5.6) for newborns, these ratios being not significantly different. Thus, at both ages, the blood is mainly supplied to the tissue by capillaries. The vascular volume attributable to large vessels generally decreases from the cortical surface to the white matter at both ages (Fig. 3D, Fig. 5C and D). However, this decrease shows a significantly different slope in newborns compared to adults, the change in the large vessel contribution being higher in adults than in newborns (Table 2, Fig. 5C and D). Thus the contribution of capillaries through the cortical depth increases more for adult than for newborn marmosets. Such observations suggest modifications in the diameter and/or the number of each type of vessel during postnatal remodeling of the vascular network. Nevertheless, neither mean vessel diameters, nor their standard deviations ($P = 0.05935$) differ between adults and newborns (Table 2).

In the comparison of *distance maps* between adults and newborns, the mode of the histogram of the distances to any vessel is exactly the same as that of small vessels for all marmosets. Hence we restrict our interest to the distance to any vessel or to any large vessel in what follows (Table 3). The mean distance to the nearest vessel is significantly smaller in adults (26.8 ± 3.8 μm) than in newborns (39.5 ± 10.1 μm) (Table 3, Fig. 4C). The higher variability in the values observed among newborn cortical samples (28–55 μm) compared to adult cortices (24–30 μm) must be noted. This variability may fit into the range of differential neuronal and tissular maturities observed among cortical areas in newborns (Conde et al., 1996; Levitt, 2003).

However, the mean distance to large vessels, although slightly higher in newborns (mean 195 ± 47.4 μm), is not significantly different from the adult mean (mean 177 ± 17.7 μm) (Table 3, Fig. 4D). Nevertheless, the total number of large vessels found in samples (Table 1) displays sample-to-sample fluctuations which might be attributed to regional variations within the cortex rather than natural fluctuations associated with finite size sampling effects. To test the possible relevance of such regional effects over fluctuations, we analyzed these values in more details.

As sample sizes are much larger than the typical large vessels separation, and as there is a high number of large vessels at the cortical surface, it is reasonable to hypothesize that the total number of large vessel distribution is Gaussian (since the sum of a large number of independent random events, here the presence of a large vessel at the cortical surface, is expected to be Gaussian—central limit theorem). In practice, the convergence toward a Gaussian distribution is generally considered to be sufficiently good when the sampling number is as small as 30, which is consistent with the data obtained in Table 1. Hence, we investigated the possible regional variability of large vessels from testing whether the total number of large vessels could be observed from the same Gaussian random variable homogeneously distributed from sample to sample (since the sampling region is the same for all samples). A Quantile–Quantile plot representation of the observed data and normal distributions gives a satisfactory linear behavior (not shown), consistently with the expected Gaussian distribution. A Kruskal–Wallis rank-test on observed data and quantiles of the Gaussian distribution at the same probability values confirms the statistical significance ($P = 0.84$) of this observation. Therefore we can conclude that the observed variations of the large vessels number in samples can be explained by sampling fluctuations, and do not necessitate the existence of additional regional variations. This is true either for adults or for newborn samples. Since we did not find any significant difference in their typical large vessel separation distance, we can conclude that large vessel neo-angiogenesis is scarce for any investigated cortical region. A more precise investigation of the literature on marmoset (Missler et al., 1993) indicates a 20% increase of cortical surface during postnatal life. The observed constant surface density of perforating vessels between newborns and adults thus implies a 20% increase in their number. Hence, remodeling of the vascular component in the cortex may occur with minor production of new perforating cortical arteries and veins since these large vessels are mainly generated during fetal life in primates (Greenberg and Jin, 2005; Norman and O'Kusky, 1986). The reduction in the distance map between newborns and adults could then be explained by a production of new small-diameter vessels. The hypothesis of a brain volume reduction inducing a reduction of the distance between vessels can be discarded since tissue volume and surface area globally increase between birth and adulthood (Fritschy and Garey, 1986; Missler et al., 1993).

Vessel/tissue distances varied linearly as a function of cortical depth and generally increased for both newborn and adult marmosets. There was a high variability in the slope between the different samples, especially in the newborn group (Table 3). However there was no significant difference in the slopes between the two ages, considering the distance either to a large vessel or to any vessel. There were only slight variations in the distances to capillaries inside the cortical tissue (Fig. 5F and H), reflecting similar exchange possibilities between tissue and blood throughout the cortical thickness.

The comparison of *segment length* between adults and newborns suggests a possible explanation other than the sprouting of small vessels for the observed increase in small vessel density in adults. The mean segment length in newborns is significantly smaller than the adult one (respectively 65.6 ± 7.6 and 90.8 ± 4.8 μm, Fig. 4B). This observation suggests that the lengthening of pre-existing vessels is partly responsible for the increase of vascular relative volume between newborn and adult marmosets. In fact, lengthening of the initial segments alone cannot sustain the increase in vascular volume: we found a significantly smaller number of segments per cubic millimeter in newborns (1844–6569) than in adults (4991–8108), indicating that new segments are slightly more than doubled during postnatal life (Table 1). The distinction between large and small vessel segments confirms that angiogenesis mainly takes place at capillary scale since 47% of the total number of vessel segments are capillaries in newborn samples when this proportion increases to 66% in adults leading to a significant difference (Table 1, $P = 0.003$). The previously mentioned analyses indicate that adult capillaries are thus twice numerous and in averaged 1.4 longer than newborn ones. From realizing that the vascular volume is proportional to both segment length and segment number, it is then straightforward to attribute the relative contribution of the observed vascular volume increase between newborn and adult age to 1/4 lengthening and 3/4 vessel creation.

4. Discussion

Using an imaging method with hitherto unrivalled resolution on elementary cerebral tissue volumes, we have been able to provide objective data on cortical vascular networks.

We have documented classic parameters. Our main purpose has however been to provide original features in the aim of reflecting the functional organization of the vessel network in the context of its relationship with the tissue: contribution of perforating vessels and capillaries to blood volume, distance map associated with the metabolic exchanges between tissue and blood, structure of the vessel pattern into segments, adaptation to increasing metabolic

needs. In order to take into consideration the high complexity of the vascular network and its variability with depth in the cortex, quantification has been obtained from the investigation of large volumes, considered as a whole or as a succession of virtual slices parallel to the cortical surface within the limit of the method resolution.

Generally speaking, angiogenesis has been particularly analyzed in two different cases: in adaptation to disturbance of the regular oxygen and nutrient supply implicated in stroke, neurodegenerative diseases, trauma or to prolonged exposure to low oxygen environments, as well as in neoplasia associated with tumor invasion and metastasis. The physiological angiogenesis occurring during normal postnatal development has been, comparatively, poorly investigated in terms of structural and functional mechanisms. However it is usually considered as an adaptation required to suit the increasing tissue needs (e.g. synaptogenesis, gliogenesis) during a period of brain size increase.

Questions arise then as to how to determine how the initial vascular pattern observed in newborn monkeys evolves to adult pattern, since characterization of some precise parameters would provide cues for understanding the role of angiogenic factors in the cascade of morphometric events required to build vascular network.

In the present conditions, relative vascular volume is doubled between newborn and adult cortex. We have quantified an increase in the contribution of capillaries to the total vascular volume through the cortical depth between newborn and adult monkeys. Moreover we have found that the increase in capillary volume is sustained both by a lengthening of pre-existing segments and, essentially, by a formation of new segments. Changes in mean capillary diameter are minor.

On the one hand, high levels of hypoxia with large and highly heterogeneous hypoxic regions, such as those found in tumors, induce remodeling with, predominantly, an increase in vessel diameter (Risser et al., 2007; Jain et al., 2007). On the other hand, for postnatal development (present study and reference work of Bär in rats (Bär, 1980)), low- or mild-intensity hypoxia (as chronic exposure to oxygen deprivation, neuronal demand due to motor learning tasks or environmental enrichment (Black et al., 1991; Isaacs et al., 1992)), structural adaptation of the cerebral vascular system induces various changes, as shown here consistently with various other studies: increase in vessel diameter, vessel density and segment length, and a decrease in inter-capillary distances (Argandoña and Lafuente, 1996; Black et al., 1991; Boero et al., 1999; Michaloudi et al., 2006; Mironov et al., 1994) after an early phase of endothelial cell hypertrophy (Harik et al., 1995).

Therefore refined tuning of the vascularization would be triggered to match the local specific needs of heterogeneous neuronal and glial cells populations presenting different delays in maturation and hypoxia susceptibility, and organized into circuits, in comparison with the predominant activity of cell multiplication in tumors. Changes in diameter and length in the micro-vascular network play a distinct role in hemo-dynamic regulation. For example, the intensification in blood flow induced by a 10% increase in diameter of a given vessel is much greater than the diminution due to a 10% level-off in its length, for a given blood pressure drop (according to Poiseuille law). Hence, to increase the efficiency of perfusion, it may be more interesting to increase vessel diameter rather than length. This might be why tumor vessels have wider but not longer vessels, in order to be able to respond to a greater metabolic demand. On the other hand, when the metabolic demand is close, as for newborn and adult tissues, the pressure drop induced by a longer vessel is much less than that induced by a similar change in diameter. Hence, the disturbance on the blood pressure distribution for a fixed metabolic demand is obtained more economically with an increase in vessel length. The pressure re-organization in a micro-vascular network due to vessel lengthening should thus be minimal in comparison with the results of a diameter change. In a mice transgenic model in which vascular volume was artificially increased through overexpression of VEGF (main angiogenic factor), it has been proposed that vascular remodeling does not occur at the individual capillary level, but results from the insertion of small vascular networks in the pre-existing vasculature (Heinzer et al., 2008). However this alternative presents functional limits since it is not associated with raises in cerebral blood flow (Vogel et al., 2004).

In conclusion, our analysis suggests that the notion of vessel density or vascular volume may not be the most relevant index to characterize the spatial distribution of the micro-vasculature. Distance maps provide better quantification of the 3D vessel distribution inside tissues, from which exchanges between blood and tissue can be better represented.

The comparative analysis between newborn and adult primates suggests a parallel between vascular development and neuronal maturation. In both cases the main features of the architecture are largely maintained between neonate and adult age whilst very important adjustment at small scale indicates a large adaptation to increasing metabolic needs. It is interesting to note that cortical maturation results in a large re-organization of both synapse population and vessel density with a high impact of angiogenesis since capillary segment number doubles between newborn and adult when synaptic density increases by 60% (Missler et al., 1993). We establish the mechanisms by which the vascular component contributes to the maturation of the cortical tissue, both in the remodeling of existing vessels and in the provision of new capillaries, especially in the innermost part of the cortex. Moreover, by analyzing different morphological parameters, we have explicitly pointed out the heterogeneity of the micro-vascularization through the cortical depth, with a high variability between different samples, signifying that these patterns may be designed by the local neuro-architectural characteristics. This observed regional variability of total vessel density should be tempered for large vessels distribution for which we found that the observed fluctuations can be explained by statistical sampling effects.

Finally the methodology which has been proposed in this study opens many substantial perspectives for a comprehensive approach of brain micro-circulation.

Acknowledgements

This work was supported by ASUPS AO3 and AO5 of Paul Sabatier University, Toulouse France; the ESRF by providing scheduled beam time; the French Ministry of Research; the ANR project BLAN06-1_142915 and the French Foundation for Medical Research (grant to LR)

The authors thank A. Steyer for his expert advice in statistical analyses and fruitful discussions and Luc Renaud for technical support.

References

Anstrom, J.A., Brown, W.R., Moody, D.M., Thore, C.R., Challa, V.R., Block, S.M., 2002. Anatomical analysis of the developing cerebral vasculature in premature neonates: absence of precapillary arteriole-to-venous shunts. Pediatr. Res. 52, 554–560.

Argandoña, E.G., Lafuente, J.V., 1996. Effects of dark rearing on the vascularization of the developmental rat visual cortex. Brain Res. 732, 43–51.

Augustin, H.G., 2001. Tubes, branches, and pillars, the many ways of forming a new vasculature. Circ. Res. 89, 645–647.

Bär, T., 1980. The vascular system of the cerebral cortex. Adv. Anat. Embryol. Cell. Biol. 59 (I–VI), 1–62.

Bell, M.A., Ball, M.J., 1985. Laminar variation in the microvascular architecture of normal human visual cortex (area 17). Brain Res. 335, 139–143.

Bertossi, M., Virgintino, D., Errede, M., Roncali, L., 1999. Immunohistochemical and ultrastructural characterization of cortical plate microvasculature in the human fetus telencephalon. Microvasc. Res. 58, 49–61.
Black, J.E., Zelazny, A.M., Greenough, W.T., 1991. Capillary and mitochondrial support of neural plasticity in adult rat visual cortex. Exp. Neurol. 111, 204–209.
Boero, J.A., Ascher, J., Arregui, A., Rovainen, C., Woolsey, T.A., 1999. Increased brain capillaries in chronic hypoxia. J. Appl. Physiol. 86, 1211–1219.
Cassot, F., Lauwers, F., Fouard, C., Prohaska, S., Lauwers-Cances, V., 2006. A novel three-dimensional computer-assisted method for a quantitative study of microvascular networks of the human cerebral cortex. Microcirculation 13, 1–18.
Carmeliet, P., 2003. Angiogenesis in health and disease. Nat. Med. 9, 653–660.
Conde, F., Lund, J.S., Lewis, D.A., 1996. The hierarchical development of monkey visual cortical regions as revealed by the maturation of parvalbumin-immunoreactive neurons. Brain Res. Dev. Brain Res. 96, 261–276.
Duvernoy, H.M., Delon, S., Vannson, J.L., 1981. Cortical blood vessels of the human brain. Brain Res. Bull. 7, 519–579.
Fonta, C., Imbert, M., 2002. Vascularization in the primate visual cortex during development. Cereb. Cortex 12, 199–211.
Fritschy, J.M., Garey, L.J., 1986. Quantitative changes in morphological parameters in the developing visual cortex of the marmoset monkey. Brain Res. Dev. Brain Res. 29, 173–188.
Greenberg, D.A., Jin, K., 2005. From angiogenesis to neuropathology. Nature 438, 954–959.
Harik, S.I., Hritz, M.A., LaManna, J.C., 1995. Hypoxia-induced brain angiogenesis in the adult rat. J. Physiol. 485 (Pt 2), 525–530.
Heinzer, S., Krucker, T., Stampanoni, M., Abela, R., Meyer, E.P., Schuler, A., Schneider, P., Muller, R., 2006. Hierarchical microimaging for multiscale analysis of large vascular networks. Neuroimage 32, 626–636.
Heinzer, S., Kuhn, G., Krucker, T., Meyer, E., Ulmann-Schuler, A., Stampanoni, M., Gassmann, M., Marti, H.H., Muller, R., Vogel, J., 2008. Novel three-dimensional analysis tool for vascular trees indicates complete micro-networks, not single capillaries, as the angiogenic endpoint in mice overexpressing human VEGF(165) in the brain. Neuroimage 39, 1549–1558.
Isaacs, K.R., Anderson, B.J., Alcantara, A.A., Black, J.E., Greenough, W.T., 1992. Exercise and the brain: angiogenesis in the adult rat cerebellum after vigorous physical activity and motor skill learning. J. Cereb. Blood Flow Metab. 12, 110–119.
Jain, R.K., di Tomaso, E., Duda, D.G., Loeffler, J.S., Sorensen, A.G., Batchelor, T.T., 2007. Angiogenesis in brain tumours. Nat. Rev. 8, 610–622.
Levitt, P., 2003. Structural and functional maturation of the developing primate brain. J. Pediatr. 143, S35–45.
Marin-Padilla, M., 1988. Embryonic vascularization of the mammalian cerebral cortex. In: Peters, A., Jones, E.G. (Eds.), Cerebral Cortex, vol. 17. Plenum Press, New York, pp. 479–509.
Michaloudi, H., Batzios, C., Grivas, I., Chiotelli, M., Papadopoulos, G.C., 2006. Developmental changes in the vascular network of the rat visual areas 17, 18 and 18a. Brain Res. 1103, 1–12.
Mironov, V., Hritz, M.A., LaManna, J.C., Hudetz, A.G., Harik, S.I., 1994. Architectural alterations in rat cerebral microvessels after hypobaric hypoxia. Brain Res. 660, 73–80.
Missler, M., Eins, S., Merker, H.J., Rothe, H., Wolff, J.R., 1993. Pre-and postnatal development of the primary visual cortex of the common marmoset. I. A changing space for synaptogenesis. J. Comp. Neurol. 333, 41–52.
Mulligan, S.J., MacVicar, B.A., 2004. Calcium transients in astrocyte endfeet cause cerebrovascular constrictions. Nature 431, 195–199.
Nishimura, N., Schaffer, C.B., Friedman, B., Lyden, P.D., Kleinfeld, D., 2007. Penetrating arterioles are a bottleneck in the perfusion of neocortex. Proc. Natl. Acad. Sci. U.S.A. 104, 365–370.
Norman, M.G., O'Kusky, J.R., 1986. The growth and development of microvasculature in human cerebral cortex. J. Neuropathol. Exp. Neurol. 45, 222–232.
Palágyi, K., Sorantin, E., Balogh, E., Kuba, A., Halmai, C., Erd''ohelyi, B., Hausseger, K., 2001. A sequential 3D thinning algorithm and its medical applications. Lect. Notes Comput. Sci. 2082, 409–415.
Peppiatt, C.M., Howarth, C., Mobbs, P., Attwell, D., 2006. Bidirectional control of CNS capillary diameter by pericytes. Nature 443, 700–704.
Pessacq, T.P., Reissenweber, N.J., 1972. Structural aspects of vasculogenesis in the central nervous system. I. Postnatal development of the capillary blood vessels. Acta Anat. (Basel) 81, 1–12.
Plouraboué, F., Cloetens, P., Fonta, C., Steyer, A., Lauwers, F., Marc-Vergnes, J.P., 2004. X-ray high-resolution vascular network imaging. J. Microsc. 215, 139–148.
Reina-De La Torre, F., Rodriguez-Baeza, A., Sahuquillo-Barris, J., 1998. Morphological characteristics and distribution pattern of the arterial vessels in human cerebral cortex: a scanning electron microscope study. Anat. Record 251, 87–96.
Risser, L., Plouraboue, F., Steyer, A., Cloetens, P., Le Duc, G., Fonta, C., 2007. From homogeneous to fractal normal and tumorous microvascular networks in the brain. J. Cereb. Blood Flow Metab. 27, 293–303.
Risser, L., Plouraboué, F., Descombes, X., 2008. Gap filling of 3-D microvascular networks by tensor voting. IEEE Trans. Med. Imaging 27, 674–687.
Stefanovic, B., Hutchinson, E., Yakovleva, V., Schram, V., Russell, J.T., Belluscio, L., Koretsky, A.P., Silva, A.C., 2008. Functional reactivity of cerebral capillaries. J. Cereb. Blood Flow Metab. 28, 961–972.
Tieman, S.B., Mollers, S., Tieman, D.G., White, J., 2004. The blood supply of the cat's visual cortex and its postnatal development. Brain Res. 998, 100–112.
Tuor, U.I., Kurpita, G., Simone, C., 1994. Correlation of local changes in cerebral blood flow, capillary density, and cytochrome oxidase during development. J. Comp. Neurol. 342, 439–448.
Vogel, J., Gehrig, M., Kuschinsky, W., Marti, H.H., 2004. Massive inborn angiogenesis in the brain scarcely raises cerebral blood flow. J. Cereb. Blood Flow Metab. 24, 849–859.
Weber, B., Keller, A.L., Reichold, J., Logothetis, N.K., 2008. The microvascular system of the striate and extrastriate visual cortex of the macaque. Cereb. Cortex 18, 2318–2330.